Extremophiles (2021) 25:115–128
https://doi.org/10.1007/s00792-021-01215-2

ORIGINAL PAPER

Characterization of a carboxylesterase with hyper-thermostability and alkali-stability from *Streptomyces lividans* TK24

Xin Chang[1] · Shuang Wu[1] · Jie Chen[1] · Shengqi Xiong[1] · Peng Wang[1] · Xueqin Shi[1] · Ao Wang[2] · Baojuan Wang[1]

Received: 18 December 2019 / Accepted: 6 January 2021 / Published online: 30 January 2021

Abstract

A gene (*estA'*, 804 bp) from *Streptomyces lividans* TK24 was artificially synthesized and successfully overexpressed as a 6His-tagged fusion protein in *Escherichia coli*. It encoded a carboxylesterase (EstA) that composed of 267 amino acids with a predicted molecular weight of 28.56 kDa. Multiple sequence alignment indicated that EstA has typical characteristics of esterases, including a catalytic triad (Ser93-Asp194-His224) and a conserved pentapeptide motif (Gly91-Leu92-Ser93-Met94-Gly95). Simultaneously, phylogenetic analysis indicated that EstA belongs to family VI. Biochemical characterization displayed its optimum enzyme activity was at 55 ℃ and pH 8.5. Additionally, EstA exhibited higher activity towards short carbon substrates and showed the outstanding catalytic efficiency for *p*NPA2 with k_{cat}/K_m of 2296.14 ± 10.35 s^{-1} mM^{-1}. Notably, EstA has hyper-thermostability and good alkali stability. The activity of EstA did not change obviously when incubated at 50 and 100 ℃ for 337 and 1 h, independently. Besides, by incubating at 100 ℃ for 6 h, EstA remained about half of its initial activity. Moreover, EstA showed stability at pH ranging from 8.0 to 11.0, and about 90% residual enzyme activity was reserved by being treated at pH 8.0 or 9.0 for 80 h, especially. Such multiple features prepare EstA for a potential candidate in the field of biological catalysis of some industrial applications under harsh conditions.

Keywords Esterase · Kinetics · Thermostability · Structural modeling

Abbreviations

*p*NP	*p*-Nitrophenol
*p*NPA2	*p*-Nitrophenyl acetate
pNPB4	*p*-Nitrophenyl butyrate
*p*NPC6	*p*-Nitrophenyl hexanoate
*p*NPC8	*p*-Nitrophenyl caprylate
*p*NPC10	*p*-Nitrophenyl decanoate
*p*NPL12	*p*-Nitrophenyl laurate
IPTG	Isopropyl-β-D-thiogalactopyranoside
SDS-PAGE	Sodium Dodecyl Sulphate–PolyAcrylamide Gel Electrophoresis
BSA	Bovine Serum Albumin
EDTA	Ethylenediaminetetraacetic acid
PMSF	Phenylmethylsulfonyl fluoride
DMSO	Dimethyl sulfoxide
DMF	Dimethylformamide
SDS	Sodium Dodecyl Sulphate
CTAB	Cetyltrimethylammonium bromide

Introduction

Esterases (EC 3.1.1.X), representing a diverse and ubiquitous group belonging to hydrolases, catalyze the formation and cleavage of ester bonds and are extensively distributed in animals, plants and microbes (Arpigny and Jaeger 1999; Bornscheuer 2002). Based on the substrate preference, they are divided into two major groups including carboxylesterases (EC 3.1.1.1) and triacylglycerol lipases (EC 3.1.1.3). Carboxylesterases prefer to accelerate the synthesis and hydrolysis of acylglycerols with relatively short-chain fatty acids (≤ 10 carbons) while lipases prefer to catalyze that

Communicated by H. Atomi.

✉ Ao Wang
syaorin@ahnu.edu.cn

✉ Baojuan Wang
wangbaojuan@ahnu.edu.cn

[1] Anhui Provincial Key Laboratory of Molecular Enzymology and Mechanism of Major Diseases and Key Laboratory of Biomedicine in Gene Diseases and Health of Anhui Higher Education Institutes, College of Life Sciences, Anhui Normal University, Wuhu 241000, Anhui, China

[2] College of Physical Education, Anhui Normal University, Wuhu 241000, Anhui, China

with long-chain (≥ 10 carbons) fatty acids (Bornscheuer 2002). Traditionally, Arpigny and Jaeger proposed dividing esterases into eight representative families depended mainly on their fundamental biological properties and the difference among their amino acid sequences (Arpigny and Jaeger 1999). As more and more microbial esterases were identified, the classification of esterases has been extended to 18 families (Samoylova et al. 2018). Furthermore, according to our recent study, the classification of esterases has been expanded to 19 families (Wang et al. 2020). As an important group of biocatalysts, esterases display more unique characteristics: high stereo-, region-, and chemo-selectivity; Besides, there is usually no cofactor required during the reaction process (Bornscheuer 2002; Ramnath et al. 2017). These advantages make esterases are widely used in biochemical, industrial, pharmaceutical and biotechnological applications (Javed et al. 2018; Panda and Gowrishankar 2005).

Most industrial processes where enzymes are utilized undergo severe conditions, for instance, high temperature and alkaline conditions. Affected by harsh reactive situations, limited ability to remain stable of enzymes with high catalytic activity has aroused demand that searching robust enzymes possessing special traits such as good thermostability and alkali stability (Bora et al. 2013; Dumorne et al. 2017). Traditionally, new enzymes have been discovered by screening cell extracts with suitable substrates (Tesch et al. 1996; Xin and Hui-Ying 2013; Yong et al. 2016). Now, companying the progressively completed genome-sequencing database and developments of bioinformatics, searching and discovering enzymes with desired properties from the predicted gene becomes an important method in industrial biocatalysts (Brault et al. 2012; Li et al. 2018; Shestakov 2012; Soror et al. 2007).

Although existing in almost all living organisms, carboxylesterases originated from microbial sources show greater importance in industrial applications than from others. *Streptomyces* is a kind of spore-forming and Gram-positive bacteria in soil, which have active secondary metabolisms and are also responsible for producing numerous commercial antibiotics and biocatalysts (van Keulen and Dyson 2014). Esterases, as the representative secondary metabolites existed widely and abundantly in *Streptomyces*, have been researched gradually. For example, an extracellular esterase was characterized from *S. diastatochromogenesa* (Tesch et al. 1996), two cold-active esterases EstB and EstC were isolated and characterized from *S. coelicolor* A3(2) (Brault et al. 2012; Soror et al. 2007), a thermostable lipase MAS1 was screened and characterized from marine *S.* sp. strain W007 (Yuan et al. 2016), two thermostable esterase EstW and EstC were identified from *S. lividans* (Wang et al. 2016, 2020) and so forth. To our knowledge, *S. lividans* TK24 contained at least 59 open reading frames (ORFs) encoded for putative esterase according to the search result in the GenBank database. However, none of these putative esterase genes but EstC with hyper-thermostability and good alkali stability has been cloned and characterized so far (Wang et al. 2020). Therefore, *S. lividans* TK24 will be an ideal resource for esterases equipped with desirable characteristics with further researches. In this study, a carboxylesterase (EstA) from *S. lividans* TK24 was classified by analysis of the phylogenetic tree and constructed to a structural model based on the template found in the PDB database. In addition, our study demonstrated successful expression of EstA in *E. coli*, purification using Co^{2+} affinity chromatography, and identification for industrial applications.

Materials and methods

Strains, plasmids and chemicals

S. lividans TK24, *Escherichia coli* (*E. coli*) DH5α, Rosetta (DE3), as well as the expression vector pET-28b(+) were maintained at – 80 ℃. The recombinant plasmid, pET-*estA'*, was synthesized artificially by Genscript (Nanjing, China). PrimeStar™ Max DNA polymerase and Co^{2+} metal affinity resin were obtained from TaKaRa (Dalian, China). Protein molecular weight standards and restriction enzymes were purchased from Thermo Fisher Scientific (Shanghai, China). Gel extraction kit and plasmid miniprep kit were gained from Axygen (California, USA). Kit of bacteria DNA was purchased from TIANGEN (Beijing, China). The *p*NP and *p*NP esters of different acyl chain lengths (*p*NPA2, *p*NPB4; *p*NPC6; *p*NPC8; *p*NPC10; *p*NPL12) were acquired from Sigma-Aldrich (St. Louis, MO, USA). Isopropyl-β-D-thiogalactopyranoside (IPTG) and bradford protein assay kit were bought from Sangon (Shanghai, China). All other chemicals were analysis reagents and used with no more purifying. Ultrapure water whose resistivity greater than 18.25 MΩ·cm was utilized by a Milli-Q Academic system (MA, USA) throughout this study.

Sequence comparison and phylogenetic analysis

Amino acid sequences of EstA with other esterases were downloaded from the National Center for Biotechnology Information (NCBI, http://www.ncbi.nlm.nih.gov/gorf/gorf.html). Similarity searches of amino acid sequences were completed by protein BLAST (http://blast.ncbi.nlm.nih.gov/) against the public GenBank database and the SignalP 4.0 server (http://www.cbs.dtu.dk/services/SignalP/) was used to predict whether EstA had a signal peptide. Multiple alignments based on secondary structure were performed by Clustal W within BioEdit and further depicted by ESPript 3.0 (http://espript.ibcp.fr/ESPript/cgi-bin/ESPript.cgi).

Mega 7.0 constructed the phylogenetic tree with 1000 replicates' bootstrap test by the Neighbor-Joining (NJ) method. The protein structure of EstA was predicted and simulated with the SWISS-MODEL (http://swissmodel.expasy.org/). Subsequently, PyMOL was used to analyze the generated three-dimensional structural model.

Construction of plasmid and strain

Containing two restriction sites: *Nde*I (forward primer underlined) and *Xho*I (reverse primer underlined), a pair of homologous primers: EstA-F' (5′- GGAATTCCATATG ATGTCAGTGTTACCGGGTGC -3′) and EstA-R' (5′- CCG CTCGAGAACCGCCGCCGGCGG -3′), was designed to amplify *estA* (Locus SLIV_RS27090) by PCR based on the *S. lividans* TK24 genomic DNA. PCR-amplification was as follows: 94 °C for 5 min, 35 cycles (94 °C for 30 s, 56 °C for 30 s, 72 °C for 1 min), 72 °C for 10 min. To construct pET-*estA*, the PCR purification digested by *Nde I* and *Xho I* was inserted into pET-28b(+). Then, pET-*estA* which verified using DNA sequencing was transformed into *E. coli* Rosetta for the heterologous expressing.

In addition, the gene named *estA'*, encoding the same amino acid sequence as *estA*, was synthesized by artificial optimization and was constructed to the plasmid pET-*estA'*. Further, pET-*estA'* was transformed into *E. coli* Rosetta and was expressed as well.

Protein expression and purification

For heterologous expression, *E. coli* Rosetta (DE3) cells encompassing recombinant plasmids (pET-*estA* or pET-*estA'*) were inoculated in the 100 mL (LB) with chloromycetin (25 μg mL^{-1}) and kanamycin (30 μg mL^{-1}) added. The culture was spun at 225 rpm and 37 ℃ until OD_{600} reached 0.5. Then, 0.1 mM IPTG was put into the culture following further culturing for 20–24 h at 20 ℃ and 180 rpm. Next, cells harvest lasted 5 min by centrifugation method at 4 ℃ and 5000 rpm. Harvested cells were broken with a Xingzhi SM-1000D ultrasonic wave cell pulverizer (Ningbo, China) on ice. In the process of cells breaking, the buffer that we selected is the mixture of 300 mM of NaCl and 50 mM of NaH_2PO_4 (pH 8.0). Subsequently, the crude enzyme liquid was centrifugated at 10,000 rpm for 20 min at 4 ℃ followed by the obtaining of the target protein (EstA) by purification of supernatant with Co^{2+} affinity chromatography. Finally, the purified protein was analyzed by 12% SDS-PAGE and determined on concentration using the Bradford method with BSA as the standard.

Determination of EstA's activities

To study EstA's activities, monitoring quantities of *p*-nitrophenol (*p*NP) discharged through esterase-catalyzed hydrolysis in 5 min at the OD_{410} using spectrophotometry. The assay of standard enzymatic activity was proceeded under the following conditions: at 25 ℃, within 1 mL volume including 10 μL diluted enzyme (0.02 mg mL^{-1}), 980 μL 50 mM Tris–HCl buffer (pH 8.5), and 10 μL 50 mM *p*NPB4. Correspondingly, the mixture contained identical composition except for the enzyme was considered as a control to determine the spontaneous hydrolysis of the substrates. It is described as one enzyme unit (U) to require a certain quantity of enzymes for producing 1 μmol of *p*NP per minute at pH 8.5 and 25 ℃. All measurements were independently performed in triplicate.

Specificities of substrates and kinetics measurements

EstA's specificities of substrates were measured at standard reaction conditions with different *p*NP esters (C2–C12) as substrates. The kinetic parameters of EstA towards *p*NPA2, *p*NPB4 and *p*NPC6 were analyzed by measuring the *p*NP release rate using different final concentrations of substrates within a range of 0.01–1 mM under the condition of standard assays. The standard curve of *p*NP release was generated by the change of absorption value with different concentrations of *p*NP at 410 nm. On this basis, the value of V_{max} and the value of K_m were calculated with the employment of the Lineweaver–Burk plots by a fitted non-linear regression transform of the initial velocity of *p*NP release versus substrate concentration. Equation $k_{cat} = V_{max}/[E]$, where $[E]$ stands for the molar concentration of EstA, was employed to determine the catalytic rate constant k_{cat} (s^{-1}).

Influences of pH and temperature on EstA

To identify the optimal pH of EstA, the study monitored enzymatic activities at a range of pH 6.0–10.5 within the following conditions: 50 mM sodium acetate, pH 6.0–7.0; 50 mM Tris–HCl, pH 7.0–9.0; and 50 mM KH_2PO_4-KOH, pH 9.0–10.5. An optimal temperature was acquired within the range of 10–65 °C using *p*NPB4 as the substrate for every interval of 5 ℃.

Thermostability and pH stability of EstA

The thermostability of EstA was detected after independent incubations of EstA at various temperatures of 10–100 ℃ for 1 h. What's more, residual activities were determined after the pre-incubation of EstA at 50 and 100 °C for various periods, respectively, under standard conditions. Subsequently,

to examine the pH stability under standard assay conditions, the residual activity of EstA was measured after incubation for a while at the pH range from 8.0 to 11.0 and 4 ℃. In all calculations, the activity of EstA without pre-incubation was 100% by default.

Impacts of metal ions and various chemical reagents on EstA

Impacts of metal ions (K^+, Fe^{2+}, Mn^{2+}, Ca^{2+}, Na^+, Zn^{2+}, Mg^{2+}, Al^{3+}, Cu^{2+}, Co^{2+}, Cr^{3+}, Hg^{2+}, Ni^{2+}) and inhibitors (PMSF; EDTA) on EstA were analyzed with different ultimate concentrations which are 1 and 10 mM. Further, the influences of organic solvents (DMSO, methanol, ethanol, isopropanol, DMF, acetonitrile, acetone) and detergents (Triton X-100, SDS, CTAB, Tween-80, Tween-20) were determined at a volume percentage (v/v) of various final concentrations of 0.1 or 1.0%, and 15 or 30%, separately. Each of reactions was performed three times independently under the optimal pH at 25 °C and the activity of EstA without treatments was 100% by default.

The circular dichroism (CD), fluorescence and UV–Vis absorption spectroscopies

To identify the effects of temperature on enzyme structure, three states of EstA, including EstA without any treatment and EstA treated, respectively, at 100 ℃ for 2 and 6 h, were analyzed by CD, fluorescence and UV–Vis spectra. Far-UV CD spectra of EstA were recorded by the Jasco-810 Circular dichroism spectrometer (Tokyo, Japan). All protein concentrations were adjusted to 0.2 mg mL^{-1} in the buffer which is a mixture of 20 mM NaH_2PO_4 and 75 mM Na_2SO_4 (pH 7.5). At 50 nm/min scan speed and a 1 nm bandwidth, the data were collected at room temperature from 190 to 280 nm using the quartz cuvette with 1 mm path length. Each sample was measured in triplicates and the mean residue ellipticity ([θ], deg cm^2 $dmol^{-1}$) was calculated by the equation as follow:

$$[\theta] = 1000 \times \frac{\text{mdeg}}{l \cdot c \cdot \text{N}}$$

Where mdeg represents for the measured CD data, l is the path length of quartz cuvette (1 mm), c stands for the protein molar concentration (mM), N represents the number of amino acid residues and the constant number 1000 stems from the conversion of the unit.

Fluorescence analysis was measured by a Shimadzu RF-5301PC spectrofluorometer (Tokyo, Japan). For monitoring changes of fluorescence, EstA was scanned at the excitation wavelength of 280 nm. The spectra were recorded in a range of 290–450 nm, excited at a slit width of 5 nm and emitted at that of 10 nm.

A UV–Vis spectrophotometer, Shimadzu UV-1700 (Tokyo, Japan), was the facility for acquiring the UV–Vis spectra of EstA. The absorbance of EstA was recorded between 200 and 800 nm according to the reading of 50 mM Tris–HCl buffer as the baseline.

Results

Sequences analysis of *estA* and *estA'*

The *estA* from *S. lividans* TK24 is an open reading frame (ORF) in a length of 804 bp. It exhibits a relatively high GC content (72.5%) which agrees with the former study that the genomic DNA of *Streptomyces* had a high GC content (Ruckert et al. 2015). Although the gene was cloned and the recombinant engineering bacteria Rosetta (DE3) pLysS/pET-*estA* was constructed successfully, the soluble expression of the *estA* in *E. coli* had not been completed due to the high GC content. For more conducive to the realization of the expression of the gene in *E. coli*, a gene named *estA',* was synthesized by artificial optimization and had been registered in the GenBank with an accession number: MN194168. Under the premise that the total length of the optimized gene sequence and the sequence of encoded amino acid remained consistent with *estA*, the artificial optimization of *estA'* was carried out by replacing the rare codons with the preferred codons of *E. coli* and decreasing the GC content from 72.5 to 54.0% (Supplementary Fig. S1).

The protein EstA which was encoded by *estA* or *estA'* has 267 amino acids. Calculated molecular weight and predicted isoelectric point of EstA was 28.56 kDa and 6.71, respectively (http://isoelectric.org/calculate.php). The result of signal peptide prediction showed that the sequence did not have any kind of signal peptide. The BioEdit analysis revealed that EstA shared sequence identities of 82.3, 76.8, 62.6 and 47.6% with esterases from *S. olindensis* (KDN75141), *S. filamentosus* NRRL 15998 (EFE73899), *S.* sp. DJ (PLW72091) and *Blastococcus* sp. CCUG 61487 (TKJ30472) in the GenBank database, respectively (Supplementary Table S1). Hence, the multiple sequence alignment analysis based on the secondary structure was performed with the above esterases from other bacteria (Fig. 1). The result showed that EstA contained a conserved catalytic triad consisted of Ser93, Asp194 and His224, and the active site Ser93 residue was located within the conserved pentapeptide motif (Gly91-Leu92-Ser93-Met94-Gly95), which is a typical characteristic commonly found in esterases (Jaeger et al. 1999).

To explore the evolutionary relationship between EstA and other known esterases, the phylogenetic analysis was

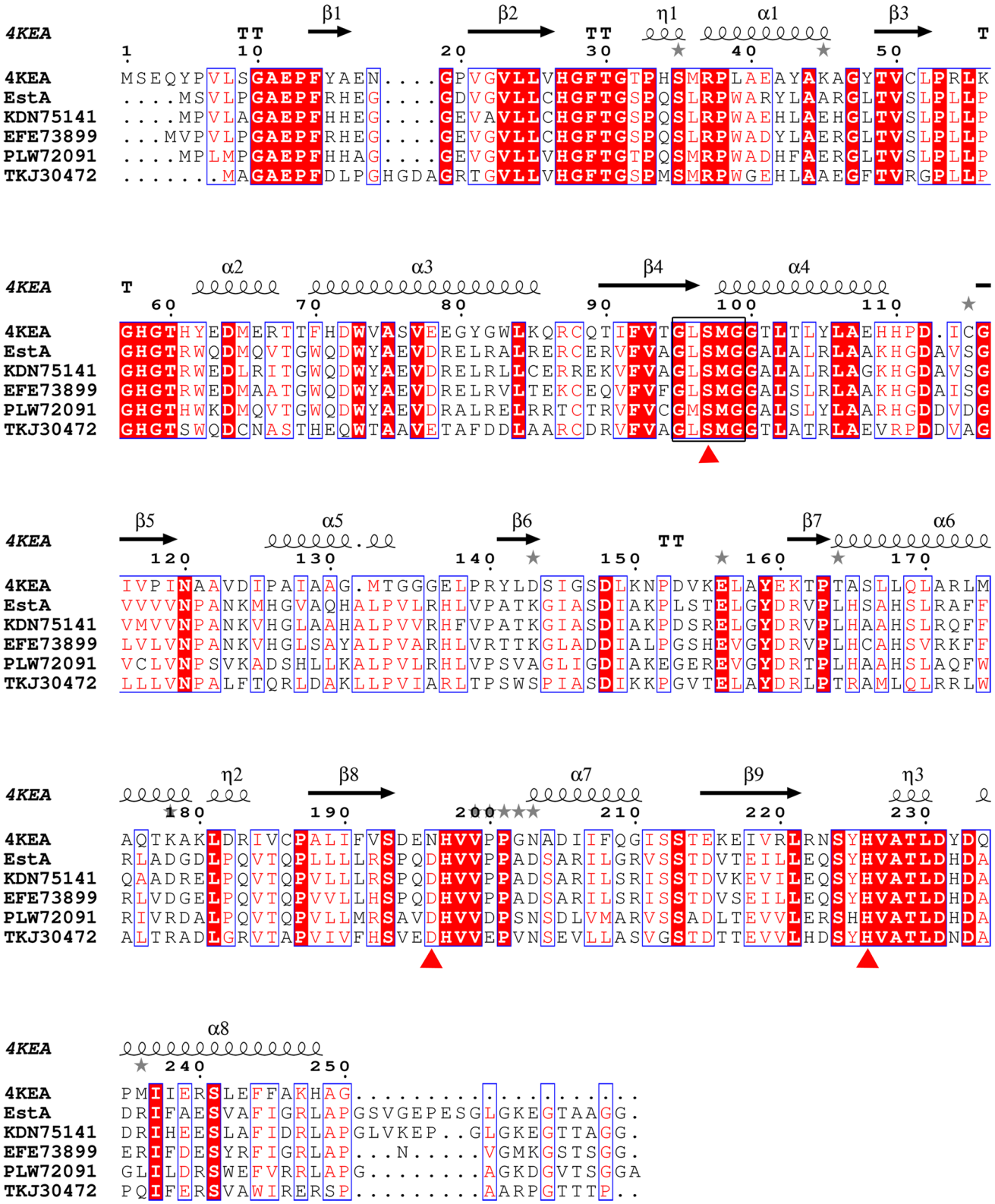

Fig. 1 Multiple sequence alignment of EstA and other related proteins. GenBank accession numbers represent as follows: 4KEA, lipase from *Bacillus* sp. H-257; KDN75141, esterase from *Streptomyces olindensis*; EFE73899, esterase from *Streptomyces filamentosus* NRRL 15,998; PLW72091, esterase from *Streptomyces* sp. DJ; TKJ30472, carboxylesterase from *Blastococcus* sp. CCUG 61,487. The alignment was carried out with Clustal W and rendered by ESPript 3.0. *Red triangles* indicate amino acids forming the catalytic triad and the conserved pentapeptide motif was *boxed* by a *black rectangle*. The alpha helix, beta sheet, random coil, and beta turn are represented by "*α*", "*β*", "*η*", and "*T*", respectively

carried out according to Arpigny and Jaeger's classical classification (Arpigny and Jaeger 1999). After alignments of EstA with the five enzymes mentioned above and other family members, the constructed phylogenetic tree demonstrated that EstA was classified as family VI (Supplementary Fig. S2). Esterases, belonging to family VI, are one of the smallest ones known and possess molecular mass ranging from 23 to 26 kDa in most cases according to Arpigny (Arpigny and Jaeger 1999). Additionally, to further clarify the relationship between EstC and family VI enzymes, another neighbor-joining phylogenetic tree was constructed using five of family VI bacterial esterase amino acid sequences proposed in the original Jaeger's paper and seven of that which had been identified and grouped in family VI to date. As depicted in Fig. 2, EstA and the five enzymes mentioned above were clustered with MHlip from Antarctic soil metagenome, once again demonstrating that EstA was a new number of this family. As shown in Table S2 in the supplementary, in terms of biochemical properties, except for R-est6, EstA and other identified family VI bacterial esterases displayed substrate specificity towards that with short carbon chains, which was consistent with the fact that all family VI esterases have the maximum activities with the small fatty acid chain esters and do not hydrolyze the long fatty acid chain esters (Soni et al. 2016). Besides, all of them severally exhibited maximum activity at a pH range of 6.5–9.0 and a temperature range 30–60 ℃. Unlike others, however, EstA showed superior thermostability and pH stability as it remained about half of its initial activity after incubation at 100 ℃ for 6 h and reserved about 90% residual enzyme activity by being treated at pH 8.0 or 9.0 for 80 h, respectively.

Structural model of EstA

A lipase (PDB code: 4KEA) used as a template was selected to create a homology model of EstA. As the Fig. 3 showed, the deduced structure adopted an α/β folding core and a partly cap region. In this whole 3D-structure of EstA, the central β-sheet composed of seven β-strands was surrounded by seven α-helices to form a spherical protein, and Ser93, Asp194, His224 gathering spatially to develop a catalytic triad positioned in a groove on the surface of the model. The other striking feature in the structure of EstA was a small 'α-helix cap', formed only four amino acid residues

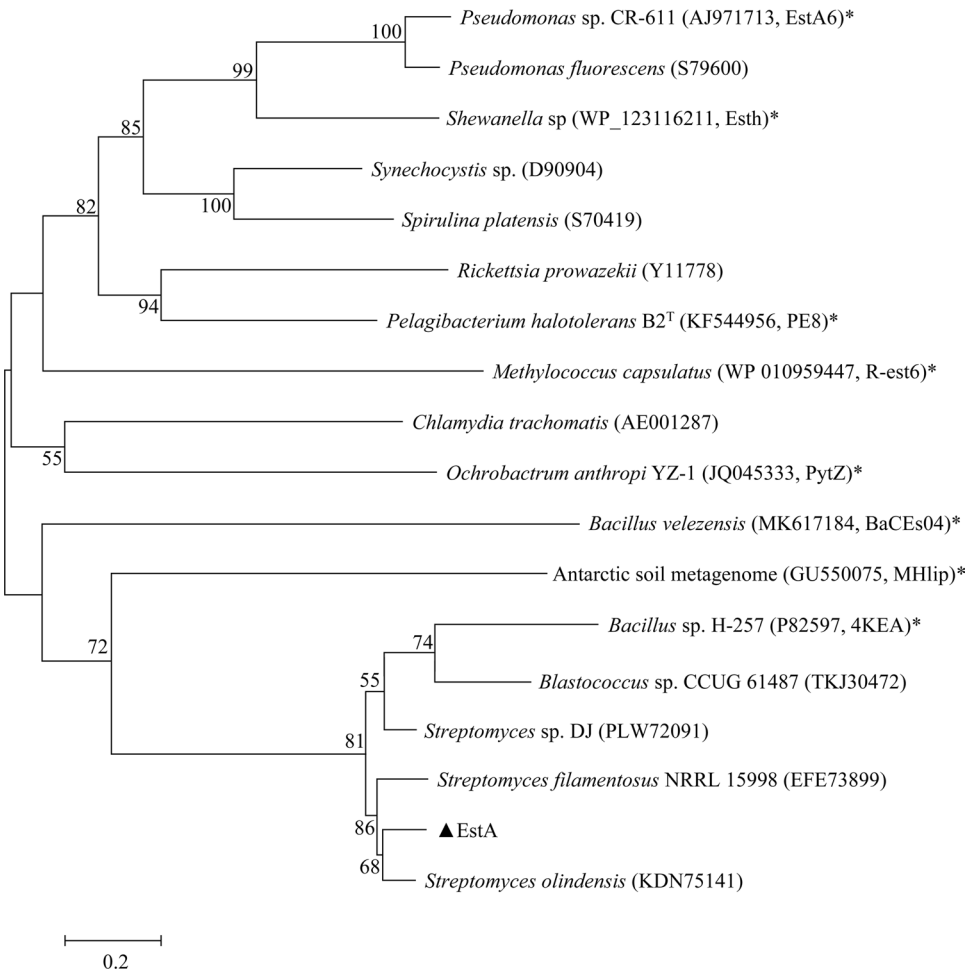

Fig. 2 Phylogenetic relationship of EstA (closed triangle) and other proteins of family VI. "*" means the experimentally characterized enzymes. The tree based on the Neighbor-Joining method was constructed by Mega 7.0 with a bootstrap test of 1000 replicates. Except for EstA, other protein sequences were retrieved from GenBank and the accession numbers of the sequences are stated in *brackets* after each enzyme. The number near every branch indicates the reliability percentage in the bootstrap test of this branch

(His123, Gly124, Val125 and Ala126), located above the catalytic triad and covered the active site (Fig. 3a). Additionally, the electrostatic potential surface of EstA was shown (Fig. 3b). The blue areas representing the positive charges and the red areas representing the negative potential almost cover equally the surface of the protein.

Expression and purification of EstA

Soluble expression of *estA* from *S. lividans* TK24 in *E. coli* Rosetta (DE3) had not been completed and the *estA'* gene synthesized artificially was successively heterogeneous expressed as a 6His-tagged fusion protein. Moreover, the homogeneity of protein was purified using Co^{2+} affinity chromatography from the crude enzyme liquid. The purifying on cell lysate using His-tag produced a purification of 4.11-fold and a 92.78% yield of activity (Supplementary Table S3). Subsequently, the purified protein exhibited a single band between 25 and 35 kDa on coomassie brilliant blue G-250 stained SDS-PAGE (12%) (Fig. 4). That proves the molecular mass of purified protein was close to the predicted one which is 28.56 kDa.

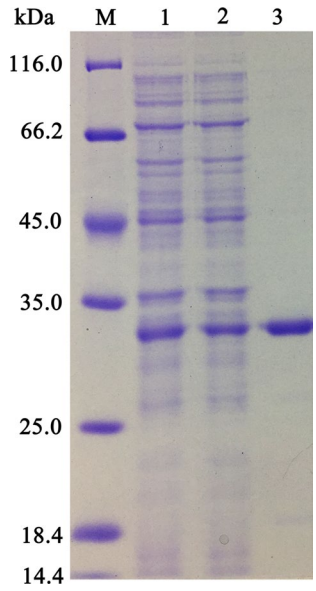

Fig. 4 SDS-PAGE analysis of EstA. Lane M: standard marker proteins; lane 1: cell lysate; lane 2: supernatant of cell lysate; lane 3: purified EstA after affinity chromatography

Determination of substrate specificities and kinetic parameters

The substrate specificity and kinetic parameters of EstA were measured using *p*NP esters with various lengths of acyl chain (C2–C12) (Table 1). The results showed that EstA displayed higher activity towards substrates with short carbon chains, such as *p*NPA2 (47.9 ± 0.7 U mg^{-1}), *p*NPB4 (31.7 ± 0.8 U mg^{-1}) and *p*NPC6 (16.1 ± 0.3 U mg^{-1}). Meanwhile, K_m values of EstA were decreased with acyl chain length (C2–C6) increasing, which corresponded with the results of substrate specificities. In addition, EstA displayed the outstanding catalytic efficiency for *p*NPA2 and *p*NPB4. Kinetic parameters (K_m, V_{max}, k_{cat}/K_m) for *p*NPA2 were 0.34 ± 0.01 mM, 16.4 ± 0.5 μM min^{-1} and 2296.1 ± 10.4 s^{-1} mM^{-1}, respectively.

Impacts of pH and temperature on the EstA

Effects of pH on EstA were studied at 25 °C with the substrate of *p*NPB4. EstA displayed a maximum of its activity at pH 8.5 while maintained greater than 50% compared with

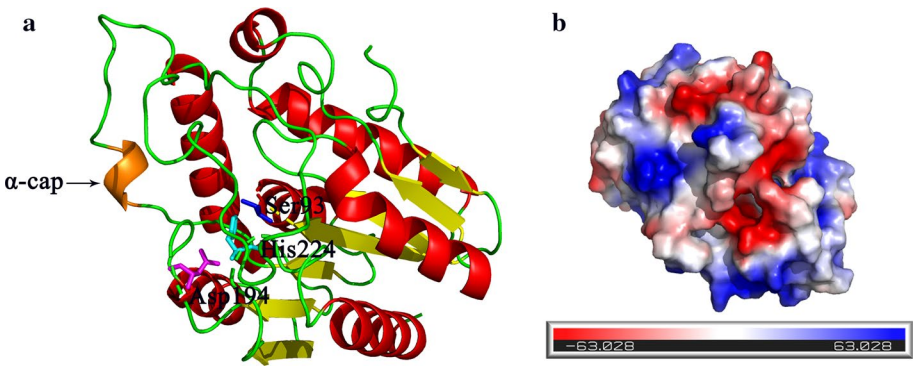

Fig. 3 The predicted structure and surface electrostatic potential analysis of EstA. **a** The EstA 3D model predicted by SWISS-MODEL with 4KEA as the template. The overall structure was composed of two main domains: an α/β hydrolase folding core and an α-helix cap. The alpha helix, beta sheet and random coil were colored in red, yellow and green, respectively. The cap region was represented in orange. The catalytic triad consisting of Ser93, Asp194 and His224 was indicated in stick representation. **b** The surface electrostatic potential of EstA analyzed by PyMOL. The cool color areas represented the positive charges and the warm color represented the negative charges

Table 1 Specific activities and kinetic parameters of EstA toward various substrates

Substrates	Specific activity (U mg^{-1}) ± SD	K_m (mM) ± SD	V_{max} (μM min^{-1}) ± SD	k_{cat} (s^{-1}) ± SD	k_{cat}/K_m (s^{-1} mM^{-1}) ± SD
*p*NPA2	47.9 ± 0.7	0.34 ± 0.01	16.4 ± 0.5	780.6 ± 24.7	2296.1 ± 10.4
*p*NPB4	31.7 ± 0.8	0.53 ± 0.05	15.3 ± 0.8	729.4 ± 36.5	1376.2 ± 13.6
*p*NPC6	16.1 ± 0.3	0.72 ± 0.09	6.2 ± 0.4	297.2 ± 18.2	412.8 ± 3.5
*p*NPC8	6.1 ± 0.6	–	–	–	–
*p*NPC10	4.4 ± 0.4	–	–	–	–
*p*NPL12	3.8 ± 0.2	–	–	–	–

"–" means no detectable

its original enzyme activity within a range of pH 7.5–9.5 (Fig. 5a). Influences of temperature on EstA were performed by detecting the hydrolysis of *p*NPB at 10–65 °C. When conducting reactions at 45–65 °C, EstA showed more than 70% of its highest activity while the highest activity was observed at 55 °C. Additionally, under the temperature of 10 ℃, EstA maintained more than 20% of its highest activity (Fig. 5b).

The thermostability and pH stability of EstA were also determined. Surprisingly, EstA displayed hyperthermostability and good alkali stability. Incubation at the temperature ranging from 10 to 100 °C for 1 h and 50 °C for 337 h hardly altered the activity of EstA (Supplementary Fig. S3). Furthermore, after incubation at 100 ℃, EstA maintained over 90% of the original activity for 2 h and it reached a half-life for about 6 h (Fig. 5c). Moreover, EstA kept good stability at a wide range of pH (from 8.0 to 11.0). This indicated that it was an alkali-stable enzyme. The enzyme activity of EstA was not changed with pre-incubated at pH 8.0–11.0 for 12 h, and it retained over 70% residual activity after 24 h. Furthermore, after incubation

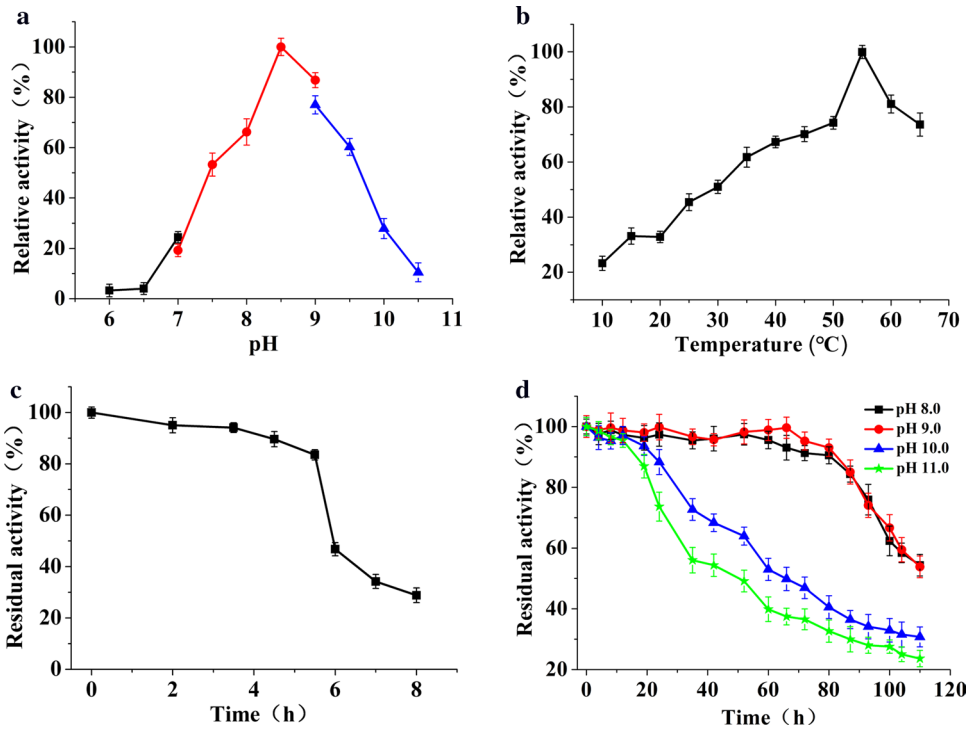

Fig. 5 Effects of pH and temperature on enzyme activity. **a** Effects of pH on EstA. The enzyme activity was measured in the following buffers at different values of pH from 6.0 to 10.5: 50 mM sodium acetate buffer (pH 6.0–7.0, black square), 50 mM Tris–HCl buffer (pH 7.0–9.0, red circle) and 50 mM KH_2PO_4-KOH buffer (pH 9.0–10.5, blue triangle). **b** Effects of temperature on EstA. The optimum temperature was measured from 10 to 60 °C in 50 mM Tris–HCl buffer (pH 8.5) and the maximum activity was defined as 100%. **c** Thermostability of EstA at 100 ℃ for 8 h. The enzyme was incubated at 100 ℃ for the indicated time and the residual activity was measured with the activity before incubation as 100%. **d** pH stability of EstA. The enzyme was incubated in various buffers with pH range from 8.0 to 11.0 (pH 8.0, black square; pH 9.0, red circle; pH 10.0, blue triangle; pH 11.0, green star) for 110 h, the activity of enzyme without any treatment was defined as 100%

for 110 h at pH 9.0 (Tris–HCl buffer), it still held almost 50% of its initial activity (Fig. 5d).

Impacts of various additives on EstA

Impacts of different metal ions and inhibitors on EstA were determined under standard assay conditions (Table 2). EstA's activity was improved in the presence of 1 mM K^+ (153.3%), Fe^{2+} (148.6%), Mn^{2+} (144.2%), Na^+ (121.8%), Ca^{2+} (109.9%) and inhibited by 1 mM Hg^{2+} (73.4%) or Ni^{2+} (70.2%). When the concentration of ions was 10 mM, the activity of EstA was still stimulated by K^+ (111.5%), Fe^{2+} (115.2%), Mn^{2+} (118.4%), Ca^{2+} (129.8%) or Mg^{2+} (109.2%) and was dramatically inhibited by Zn^{2+} (35.2%), Cu^{2+} (34.4%) or Ni^{2+} (10.2%). The activity of EstA had little effect by EDTA (1 and 10 mM) or PMSF (1 mM), but it was inhibited 27.4% by PMSF at 10 mM.

Additionally, EstA was slightly affected by all detected detergents at 0.1% concentration and strongly inhibited at 1.0% concentration by Span-20 (30.8%), SDS (35.6%) and CTAB (44.2%) (Table 3). Furthermore, the reaction mixture was added with various organic solvents to assess their influence on enzyme activity with a final concentration of 15 or 30% (Table 4). EstA was relatively stable in DMSO, ethanol, methanol, DMF, and was inhibited obviously in the presence of 30% acetone (48.3%) or acetonitrile (29.6%).

Table 2 Effects of metal ions and inhibitors on the activity of EstA[a]

Compounds	Relative activity (%±SD) (1 mM)	Relative activity (%±SD) (10 mM)
Control	100.0±0.5	100.0±0.5
K^+ (KCl)	153.3±3.1	111.5±2.5
Fe^{2+} (FeSO4)	148.6±2.0	115.2±2.2
Mn^{2+} ($MnCl_2$)	144.2±5.3	118.4±3.2
Na^+ (NaCl)	121.8±4.1	100.9±2.3
Ca^{2+} ($CaCl_2$)	109.9±4.7	129.8±3.1
Zn^{2+} ($ZnSO_4$)	103.7±4.3	35.2±4.4
Mg^{2+} ($MgCl_2$)	100.3±1.2	109.2±1.7
Cu^{2+} ($CuSO_4$)	93.4±1.1	34.4±1.9
Al^{3+} ($AlCl_3$)	89.5±2.3	55.8±2.6
Co^{2+} ($CoCl_2$)	88.7±5.7	54.8±2.8
Cr^{3+} ($CrCl_3$)	82.2±1.4	54.4±2.1
Hg^{2+} ($HgCl_2$)	73.4±1.6	50.7±1.7
Ni^{2+} ($NiSO_4$)	70.2±0.8	10.2±1.5
EDTA	99.5±4.7	96.0±3.6
PMSF	97.42±3.2	72.6±5.6

[a]Effects of metal ions on EstA were determined in the standard system with various metal ions of different concentrations (1 and 10 mM). The control was treated in the standard system without the addition of any metal ions

Table 3 The diverse sensitivities of EstA on different detergents[a]

Detergents	Relative activity (%±SD) (0.1% (v/v))	Relative activity (%±SD) (1.0% (v/v))
Control	100.0±0.5	100.0±0.5
Span-20	97.3±2.7	30.8±1.9
Tween-20	113.0±3.6	107.4±4.9
SDS	104.4±2.0	35.6±1.1
Triton X-100	101.0±2.1	82.2±2.0
Tween-80	90.8±4.6	84.3±6.2
CTAB	89.7±0.7	44.2±2.4

[a]Effects of detergents on EstA were measured in the standard system with various detergents of different concentrations (0.1 and 1.0% (v/v)). The control was treated in the standard system without the addition of any detergents

The analyses of CD, fluorescent changes and variations of UV–Vis spectra

Effects of temperature on EstA's structure were examined by measuring the changes of CD, fluorescence and UV–Vis spectroscopies. As for CD spectrums of untreated EstA, there was a positive peak at 193 nm and two negative spikes at 208 and 220 nm separately, which signifies a typical mixed α/β folding structure (Batumalaie et al. 2018). After incubation at 100 ℃ for 2 h, there was no significant change in the direction of the curve and peak positions, indicating that the native structural conformation and functionality were retained. However, when incubation time increased to 6 h, an obvious reduction of signal intensity occurred at 193 nm. In addition, two spikes of negative ellipticity were observed to shift to 200 and 215 nm, respectively (Fig. 6a).

Table 4 The influences of different organic solvents on the enzyme activity of EstA[a]

Organic solvents	Log*P*[b]	Relative activity (%±SD) (15% (v/v))	Relative activity (%±SD) (30% (v/v))
Control	–	100.0±0.5	100.0±0.5
DMSO	− 1.22	100.8±1.7	96.6±5.2
Ethanol	− 0.31	91.7±7.7	74.1±7.9
Methanol	− 0.76	88.0±0.9	73.1±2.3
DMF	− 1.01	87.2±6.0	85.3±3.9
Acetonitrile	− 0.33	67.4±0.9	29.6±0.8
Acetone	− 0.23	63.9±0.3	48.3±8.2

[a]Effects of organic solvents on EstA were tested in the standard system with various organic solvents of different concentrations (15 and 30% (v/v)). The control was treated in the standard system without the addition of any organic solvents

[b] Log*P*, the logarithm of the partition coefficient, is represented as a quantitative measure of the polarity

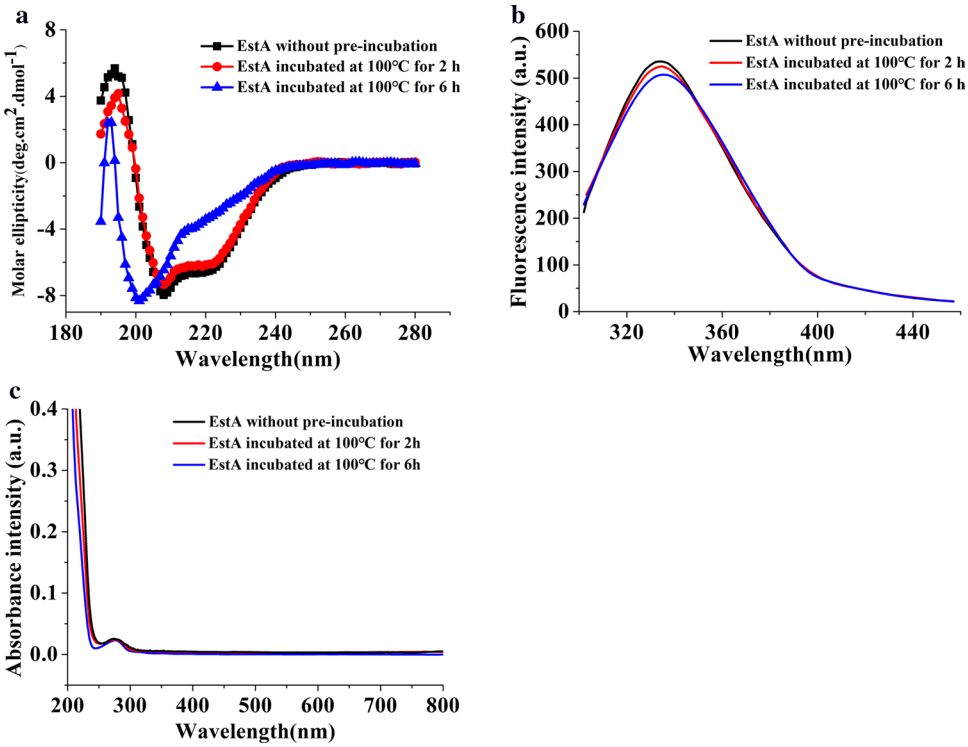

Fig. 6 Structural analysis of EstA after pre-incubation at 100 ℃ for 2 and 6 h. **a** The Circular dichroism (CD) spectra of EstA. **b** The fluorescence emission spectra of EstA. **c** The UV–Vis spectra of EstA. All measurements were carried out in triplicate independently

These results indicated that there was an apparent alternation of the secondary structure of EstA after heat treatment at 100 ℃ for 6 h compared to the intrinsic CD spectra, which was consistent with the conclusions of thermostability measurements.

For fluorescence and UV–Vis spectra, the absorption peaks are caused by individual amino acids. The maximum intensity on fluorescence and UV–Vis spectroscopies were detected at 340 and 280 nm when EstA in the native state, respectively. After incubation at 100 ℃ for 2 or 6 h, little shift of λ_{max} and a decline of intensity on fluorescence spectra were observed (Fig. 6b), on the other hand, the UV–Vis spectra also showed no changes in intensity and λ_{max} (Fig. 6c). Hence, as the heating time increased, the structure of EstA may be damaged to some extent, but the amino acid sequence as the primary structure remained stable.

Discussion

In our research, *estA* from *S. lividans* TK24 was successfully optimized and overexpressed in *E. coli*. The encoded protein (EstA) was characterized on substrates specificity, thermostability, alkali stability and influences of various additives, respectively. On the performance of substrates, EstA showed the highest affinity towards *p*NPA2 with a K_m of 0.34 mM and the affinity for substrates declined along with the increase of carbon chain length by degrees. Beyond that, there was almost no enzyme activity detected when the length of carbon chains was greater than 10. So, we defined EstA as a carboxylesterase instead of a lipase.

The effects of various additives on EstA may be due to the fact of their binding to the certain binding sites which are on the surface of the molecular and changing catalytic property of the enzyme itself (Guncheva and Zhiryakova 2011). As for metal ions, EstA was activated by several metal cations such as K^+, Fe^{2+}, Mn^{2+} or Ca^{2+}, in which K^+, Fe^{2+} and Mn^{2+} exhibited higher increases. Similar enhancement of K^+ and Mn^{2+} were observed in the Est903 located in a metagenomic library of paper mill sludge (Jia et al. 2019) and the lipase from *Bacillus* sp. VITL8 (Balaji and Jayaraman 2014), respectively. In most studies, Fe^{2+} was found to inhibit enzyme activities. Nevertheless, there are also a few esterases that can be activated in the presence of Fe^{2+}. For instance, the enzyme activities of EstAS from activated sludge metagenome (Zhang and Han 2010) and EstUT1 from *Ureibacillus thermosphaericus* (Samoylova et al. 2018) were increased up to 104% by 1 mM Fe^{2+} and 152% by 10 mM Fe^{2+}, respectively. Generally, Ca^{2+} was reported to be critical for enzyme activity. For example, the activities of lipase from *Bacillus* sp. strain L2 (Sabri et al. 2009) and LipS2 from *Chromohalobacter canadensis* (Ai et al. 2018) were increased fivefold and 57% in the presence

of Ca^{2+}, independently. For metal chelator, EstA is not a metal ion-dependent enzyme, as proven by that EDTA had few inhibitions on enzyme activity, corresponding with the fact that cofactors are not required in catalysis of EstC and EstW (Wang et al. 2016, 2020). Organic solvents and detergents which were detected in this study almost inhibited the activity of EstA in different degrees. This feature varies from that of lipase, which is usually switched on by detergents or organic solvents through enhancing access between the substrate and the hydrophobic binding site (Priyanka et al. 2019).

In terms of the predicted structure, the protein core of EstA employed a representative α/β hydrolase fold. Unlike a canonical fold composed of eight parallel β-strands, the central β-sheet of EstA only consisted of seven β-strands. There are analogous deviations that come from the canonical α/β hydrolase fold existing in LipA from *Bacillus subtilis* (van Pouderoyen et al. 2001) and MAS1 from *S.* sp. strain W007 (Yuan et al. 2016). A serine residue as a common feature of most esterases usually locates at the enzyme's binding site, which causes enzymatic activities can be affected by serine inhibitors such as PMSF. Nonetheless, in this study, due to the presence of the 'α-helix cap', EstA was only slightly inhibited by PMSF even at a concentration of 10 mM. In fact, the cap region may keep the inhibitor from the enzyme's active site, and this mechanism has been reported from a *Pseudomonas aeruginosa* lipase (Gaur et al. 2008) and a marine sediment esterase Lip3 (De Santi et al. 2016).

Generally, thermostability esterases have a broad prospect on applications with the basis of longer working life and better tolerance even in an extreme environment. In this study, the optimal temperature of EstA was 55 ℃ and the enzyme activity not only had no significant change after incubated at 50 ℃ for 337 h, but about 80% relative activity can also be maintained after the incubation at 100 ℃ for 4 h. Compared with some recently reported thermostability esterases (Table 5), the performance of EstA was better than E34Tt from *Thermus thermophilus* HB27 (Fuciños et al. 2011), EstDZ2 from a hot spring (Zarafeta et al. 2016), two lipases (ThLip1 and ThLip2) from *Thermoanaerobacterium thermosaccharolyticum* (Li et al. 2018), Est5250 from *Bacillus thermocloaceae* (Yang et al. 2019), EstW from *S. lividans* TK64 (Wang et al. 2016) and EstC from *S. lividans* TK24 (Wang et al. 2020). Additionally, many industrial applications are also performed under alkaline conditions. The most commercially important application of esterases is their addition to detergents due to their ability to remove fat stains and oil or fatty deposits from clothes in alkaline conditions. Simultaneously, esterases employed in the leather industry are mainly attributed to their ability to remove fats and grease from skins and hides in alkaline conditions. Consequently, for esterases, the alkali-stability is an especially important feature for their applications in the detergent and leather industry. In this study, EstA was highly active at pH 8.5 and showed good tolerance against alkaline conditions. The enzyme remained steady at the pH from 8.0 to 11.0. Furthermore, it even maintained over 90% activity compared with the original one after incubating for 80 h at pH 9.0, which was superior to most reported alkali-stable esterases, such as Est700 from *Bacillus licheniformis* (Zhang et al. 2018) and AMS8 from *Antarctic Pseudomonas* (Ganasen et al. 2016). Notably, compared with other esterases that are both thermostable and alkali-stable, EstA also had an advantage over MAS1 from *Streptomyces* (Yuan et al. 2016), an extracellular esterase from *Bacillus cereus* strain AGP-03 (Ghati and Paul 2015), Est903 from paper mill sludge (Jia et al. 2019) and EstC from *S. lividans* TK24 (Wang et al. 2020).

Furthermore, high catalytic efficiency is also essential for esterases on industrial applications. The specific activity of EstA towards short-chain esters (C2, 47.9 U mg^{-1}; C4, 31.7 U mg^{-1}; C6, 16.1 U mg^{-1}) was greater than that of most thermostable esterases, such as Est-XG2 from the metagenomic library (Shao et al. 2013) (C2, 39.6 U mg^{-1}; C4, 17.7 U mg^{-1}; C6, 12.2 U mg^{-1}) and EstW from *S. lividans* TK64 (Wang et al. 2016) (C2, 7.6 U mg^{-1}; C4, 4.7 U mg^{-1}; C6, 1.1 U mg^{-1}). Additionally, k_{cat}/K_m value represents the catalytic efficiency of an enzyme at low substrate concentrations, it is generally used to objectively compare the catalytic efficiency of different enzymes. In this study, kinetic parameters of EstA were performed using the following substrates: *p*NPA2, *p*NPB4 and *p*NPC6, and the k_{cat}/K_m of EstA showed the highest value towards *p*NPA2 (2296.1 s^{-1} mM^{-1}), which was consistent with the substrate specificity results. The value was also higher than most of thermostable esterases, such as EstC (1923.4 s^{-1} mM^{-1} for *p*NPA2) from *S. lividans* TK24 (Wang et al. 2020), Est5250 (1004.3 s^{-1} mM^{-1} for *p*NPA2) from *Bacillus thermocloaceae* (Yang et al. 2019) and Est903 (914.6 s^{-1} mM^{-1} for *p*NPB4) from a metagenomic library of paper mill sludge (Jia et al. 2019).

In conclusion, a carboxylesterase EstA from *S. lividans* TK24 being a member of family VI was successfully expressed and characterized. Under the condition of 55 °C and pH 8.5, EstA displayed maximum activity. On performances of substrates, EstA displayed outstanding catalytic efficiency for short-chain *p*NP esters (C2–C6), especially for *p*NPA2. Notably, EstA showed some attractive properties including hyper-thermostability and good alkali stability. The enzyme activity of EstA did not significantly fail after being incubated at 50 ℃ and pH 9.0 for 337 and 80 h, respectively. Such characteristics make EstA potential for various basic researches as well as industrial applications.

Table 5 Esterases with thermostability and pH stability identified from bacteria

Organism	Protein	pH Opt	Tem. Opt. (℃)	Thermostability	pH stability	Reference
Streptomyces lividans TK24	EstA	8.5	55	Maintained relatively stable at 55 °C × 337 h and 80% residual activity at 100 °C × 4 h	Maintained > 90% relative activity at pH 9.0 × 80 h	This study
Streptomyces lividans TK24	EstC	9	55	Maintained highest enzyme activity at 55 °C × 100 h and > 95% residual activity at 100 °C × 1 h	Remained about 90% residual activity at pH 8.0 or 9.0 × 26 h	Wang et al. (2020)
Thermus thermophilus HB27	E34Tt	6.3	58	Half-life of 107.9 min at 85 °C	–	Fuciños et al. (2011)
A metagenomic sample collected from a hot spring	EstDZ2	8.0	55	Half-life of > 6 h at 60 °C	–	Zarafeta et al. (2016)
Thermoanaerobacterium thermosaccharolyticum	ThLip1	6.5	80	Maintained > 70% of initial activity from 70 to 85 °C × 2 h	–	Li et al. (2018)
Bacillus thermocloaceae	ThLip2	6.5	75	Retained almost 95% of initial activity at 65 °C × 2 h	–	Yang et al. (2019)
	Est5250	8.0	60	Retained > 60% of its original activity × 12 h at 60 °C in the presence of Ca^{2+}	–	
Streptomyces lividans TK64	EstW	8.0	50	Half-life of 12.5 h at 95 ℃	–	Wang et al. (2016)
Bacillus licheniformis	Est700	8.0	30	–	Remained about 90% relative activity after incubation at pH 5.0–11.0 × 12 h	Zhang et al. (2018)
Pseudomonas	AMS8	10.0	30	–	Retained > 50% of its relative activity at pH 4.0–12.0 × 30 min	Ganasen et al. (2016)
Streptomyces sp.strain W007	MAS1	7.0	40	Retained > 80% of initial activity at 60 °C × 1 h and a half-life of 8.7 min at 70 °C	Maintained relatively stable at pH 6.0–9.0 × 12 h	Yuan et al. (2016)
Bacillus cereus strain AGP-03	An extracellular esterase	8.5	55	Retained > 50% residual activity after pre-incubation at the temperature range of 30–70 ℃ × 2 h	Retained > 75% residual activity after pre-incubation at pH 5.5–10.0 × 24 h	Ghati and Paul (2015)
Obtained from paper mill sludge	Est903	9.0	51	> 50% residual activity was maintained after incubation below 50 °C × 1.5 h	Maintained > 50% residual activity after incubation at pH 6.0–10.0 × 5 h	Jia et al. (2019)

"–" means no description in the corresponding literature

Supplementary Information The online version contains supplementary material available at https://doi.org/10.1007/s00792-021-01215-2.

Acknowledgments To start with, we would like to admit that, without the support of the National Natural Science Foundation of China (31400003, 31600167), this work could not have been accomplished. Next, Thanks also go to the Nature Science Foundation of Anhui Province (1608085MC67), the Provincial Project of Natural Science Research for Colleges and Universities of Anhui Province of China (KJ2016A274, KJ2019A0498), and the Postgraduate Research Innovation Program of Anhui Normal University (2019kycx055). In addition, we would like to keep a special appreciated note to the Innovation Team of Scientific Research Platform owned by Anhui Universities. Finally, I was deeply honored by getting hold of the supporting from Anhui Provincial Key Laboratory of the Conservation and Exploitation of Biological Resources.

Author contributions All authors contributed to the study conception and design. Material preparation and experiments were performed by XC, SW, AW, JC and SX. The data collection and analysis were performed by BW, AW, XC, SW, PW, and XS. The first draft of the manuscript was written by BW, AW, XC and SW, and all authors commented on previous versions of the manuscript. All authors read and approved the final manuscript.

Compliance with ethical standards

Conflict of interest The authors declare that they have no conflict of interest.

References

Ai L, Huang Y, Wang C (2018) Purification and characterization of halophilic lipase of *Chromohalobacter* sp. from ancient salt well. J Basic Microbiol 58:647–657. https://doi.org/10.1002/jobm.201800116

Arpigny JL, Jaeger KE (1999) Bacterial lipolytic enzymes: classification and properties. Biochem J 343:177–183

Balaji L, Jayaraman G (2014) Metal ion activated lipase from halotolerant *Bacillus* sp. VITL8 displays broader operational range. Int J Biol Macromol 67:380–386. https://doi.org/10.1016/j.ijbiomac.2014.03.050

Batumalaie K, Khalili E, Mahat NA, Huyop F, Wahab RA (2018) Biophysical characterization of a recombinant lipase KV1 from *Acinetobacter haemolyticus* in relation to pH and temperature. Biochimie 152:198–210. https://doi.org/10.1016/j.biochi.2018.07.011

Bora L, Gohain D, Das R (2013) Recent advances in production and biotechnological applications of thermostable and alkaline bacterial lipases. J Chem Technol Biotechnol 88:1959–1970. https://doi.org/10.1002/jctb.4170

Bornscheuer UT (2002) Microbial carboxyl esterases: classification, properties and application in biocatalysis. FEMS Microbiol Rev 26:73–81. https://doi.org/10.1111/j.1574-6976.2002.tb00599.x

Brault G, Shareck F, Hurtubise Y, Lepine F, Doucet N (2012) Isolation and characterization of EstC, a new cold-active esterase from *Streptomyces coelicolor* A3(2). PLoS ONE 7:e32041. https://doi.org/10.1371/journal.pone.0032041

De Santi C, Altermark B, Pierechod MM, Ambrosino L, de Pascale D, Willassen NP (2016) Characterization of a cold-active and salt tolerant esterase identified by functional screening of Arctic metagenomic libraries. BMC Biochem 17:1–13. https://doi.org/10.1186/s12858-016-0057-x

Dumorne K, Cordova DC, Astorga-Elo M, Renganathan P (2017) Extremozymes: a potential source for industrial applications. J Microbiol Biotechnol 27:649–659. https://doi.org/10.4014/jmb.1611.11006

Fuciños P, Pastrana L, Sanromán A, Longo MA, Hermoso JA, Rúa ML (2011) An esterase from *Thermus thermophilus* HB27 with hyper-thermoalkalophilic properties: purification, characterisation and structural modelling. J Mol Catal B Enzym 70:127–137. https://doi.org/10.1016/j.molcatb.2011.02.017

Ganasen M, Yaacob N, Rahman RN, Leow AT, Basri M, Salleh AB, Ali MS (2016) Cold-adapted organic solvent tolerant alkalophilic family I.3 lipase from an Antarctic *Pseudomonas*. Int J Biol Macromol 92:1266–1276. https://doi.org/10.1016/j.ijbiomac.2016.06.095

Gaur R, Gupta A, Khare SK (2008) Purification and characterization of lipase from solvent tolerant *Pseudomonas aeruginosa* PseA. Process Biochem 43:1040–1046. https://doi.org/10.1016/j.procbio.2008.05.007

Ghati A, Paul G (2015) Purification and characterization of a thermohalophilic, alkali-stable and extremely benzene tolerant esterase from a thermo-halo tolerant *Bacillus cereus* strain AGP-03, isolated from 'Bakreshwar' hot spring, India. Process Biochem 50:771–781. https://doi.org/10.1016/j.procbio.2015.01.026

Guncheva M, Zhiryakova D (2011) Catalytic properties and potential applications of *Bacillus* lipases. J Mol Catal B Enzym 68:1–21. https://doi.org/10.1016/j.molcatb.2010.09.002

Jaeger KE, Dijkstra BW, Reetz MT (1999) Bacterial biocatalysts: molecular biology, three-dimensional structures, and biotechnological applications of lipases. Annu Rev Microbiol 53:315–351. https://doi.org/10.1146/annurev.micro.53.1.315

Javed S, Azeem F, Hussain S, Rasul I, Siddique MH, Riaz M, Afzal M, Kouser A, Nadeem H (2018) Bacterial lipases: a review on purification and characterization. Prog Biophys Mol Biol 132:23–34. https://doi.org/10.1016/j.pbiomolbio.2017.07.014

Jia ML, Zhong XL, Lin ZW, Dong BX, Li G (2019) Expression and characterization of an esterase belonging to a new family via isolation from a metagenomic library of paper mill sludge. Int J Biol Macromol 126:1192–1200. https://doi.org/10.1016/j.ijbiomac.2019.01.025

Li W, Shi H, Ding H, Wang L, Zhang Y, Li X, Wang F (2018) Characterization of two novel thermostable esterases from *Thermoanaerobacterium thermosaccharolyticum*. Protein Expr Purif 152:64–70. https://doi.org/10.1016/j.pep.2018.04.010

Panda T, Gowrishankar BS (2005) Production and applications of esterases. Appl Microbiol Biotechnol 67:160–169. https://doi.org/10.1007/s00253-004-1840-y

Priyanka P, Tan Y, Kinsella GK, Henehan GT, Ryan BJ (2019) Solvent stable microbial lipases: current understanding and biotechnological applications. Biotechnol Lett 41:203–220. https://doi.org/10.1007/s10529-018-02633-7

Ramnath L, Sithole B, Govinden R (2017) Classification of lipolytic enzymes and their biotechnological applications in the pulping industry. Can J Microbiol 63:179–192. https://doi.org/10.1139/cjm-2016-0447

Ruckert C, Albersmeier A, Busche T, Jaenicke S, Winkler A, Friethjonsson OH, Hreggviethsson GO, Lambert C, Badcock D, Bernaerts K, Anne J, Economou A, Kalinowski J (2015) Complete genome sequence of *Streptomyces lividans* TK24. J Biotechnol 199:21–22. https://doi.org/10.1016/j.jbiotec.2015.02.004

Sabri S, Rahman RN, Leow TC, Basri M, Salleh AB (2009) Secretory expression and characterization of a highly Ca^{2+}-activated thermostable L2 lipase. Protein Expr Purif 68:161–166. https://doi.org/10.1016/j.pep.2009.08.002

Samoylova YV, Sorokina KN, Romanenko MV, Parmon VN (2018) Cloning, expression and characterization of the esterase estUT1 from *Ureibacillus thermosphaericus* which belongs to a new

lipase family XVIII. Extremophiles 22:271–285. https://doi.org/10.1007/s00792-018-0996-9

Shao H, Xu L, Yan Y (2013) Isolation and characterization of a thermostable esterase from a metagenomic library. J Ind Microbiol Biotechnol 40:1211–1222. https://doi.org/10.1007/s10295-013-1317-z

Shestakov SV (2012) Impact of metagenomics on biotechnological development. Appl Biochem Microl 48:705–715. https://doi.org/10.1134/s0003683812090050

Soni S, Odaneth AA, Lali AM, Chandrayan SK (2016) Expression, purification and biochemical characterization of a family 6 carboxylesterase from *Methylococcus capsulatus (bath)*. Protein Expres Purif 122:31–37. https://doi.org/10.1016/j.pep.2016.02.007

Soror SH, Verma V, Rao R, Rasool S, Koul S, Qazi GN, Cullum J (2007) A cold-active esterase of *Streptomyces coelicolor* A3(2): from genome sequence to enzyme activity. J Ind Microbiol Biotechnol 34:525–531. https://doi.org/10.1007/s10295-007-0224-6

Tesch C, Nikoleit K, Gnau V, Gotz F, Bormann C (1996) Biochemical and molecular characterization of the extracellular esterase from *Streptomyces diastatochromogenes*. J Bacteriol 178:1858–1865. https://doi.org/10.1128/jb.178.7.1858-1865.1996

Keulen GV, Dyson PJ (2014) Production of specialized metabolites by *Streptomyces coelicolor* A3(2). Adv Appl Microbiol 89:217–266. https://doi.org/10.1016/B978-0-12-800259-9.00006-8

Pouderoyen GV, Eggert T, Jaeger KE, Dijkstra BW (2001) The crystal structure of *Bacillus subtilis* lipase: a minimal alpha/beta hydrolase fold enzyme. J Mol Biol 309:215–226. https://doi.org/10.1006/jmbi.2001.4659

Wang B, Wang A, Cao Z, Zhu G (2016) Characterization of a novel highly thermostable esterase from the Gram-positive soil bacterium *Streptomyces lividans* TK64. Biotechnol Appl Biochem 63:334–343. https://doi.org/10.1002/bab.1465

Wang B, Wu S, Chang X, Chen J, Ma J, Wang P, Zhu G (2020) Characterization of a novel hyper-thermostable and chlorpyrifos-hydrolyzing carboxylesterase EstC: a representative of the new esterase family XIX. Pestic Biochem Phys 170:104704. https://doi.org/10.1016/j.pestbp.2020.104704

Xin L, Yu H (2013) Purification and characterization of an extracellular esterase with organic solvent tolerance from a halotolerant isolate, Salimicrobium sp. LY19. BMC Biotechnol 13:108. https://doi.org/10.1186/1472-6750-13-108

Yang Y, Ghatge S, Hur HG (2019) Characterization of a novel thermostable carboxylesterase from thermoalkaliphilic bacterium *Bacillus thermocloaceae*. Biosci Biotechnol Biochem 83:882–891. https://doi.org/10.1080/09168451.2019.1574555

Yong SK, Lim BH, Saleh S, Tey L-H (2016) Optimisation, purification and characterisation of extracellular lipase from *Botryococcus sudeticus* (UTEX 2629). J Mol Catal B Enzym 126:99–105. https://doi.org/10.1016/j.molcatb.2016.02.004

Yuan D, Lan D, Xin R, Yang B, Wang Y (2016) Screening and characterization of a thermostable lipase from marine *Streptomyces* sp. strain W007. Biotechnol Appl Biochem 63:41–50. https://doi.org/10.1002/bab.1338

Zarafeta D, Moschidi D, Ladoukakis E, Gavrilov S, Chrysina ED, Chatziioannou A, Kublanov I, Skretas G, Kolisis FN (2016) Metagenomic mining for thermostable esterolytic enzymes uncovers a new family of bacterial esterases. Sci Rep 6:38886. https://doi.org/10.1038/srep38886

Zhang T, Han W (2010) Gene cloning and characterization of a novel esterase from activated sludge metagenome. Microb Cell Fact 8:67. https://doi.org/10.1186/1475-2859-9-25

Zhang W, Xu H, Wu Y, Zeng J, Guo Z, Wang L, Shen C, Qiao D, Cao Y (2018) A new cold-adapted, alkali-stable and highly salt-tolerant esterase from *Bacillus licheniformis*. Int J Biol Macromol 111:1183–1193. https://doi.org/10.1016/j.ijbiomac.2018.01.152